JOC The Journal of Organic Chemistry

Article

pubs.acs.org/joc

Mechanism and Site Selectivity in Visible-Light Photocatalyzed C−H Functionalization: Insights from DFT Calculations

Taye B. Demissie[†,‡] and Jørn H. Hansen*[,‡]

[†]Centre for Theoretical and Computational Chemistry, [‡]Department of Chemistry, UiT The Arctic University of Norway, N-9037 Tromsø, Norway

Supporting Information

ABSTRACT: Visible-light photocatalyzed (VLPC) late-stage C−H functionalization is a powerful addition to the chemical synthesis toolkit. VLPC has a demonstrated potential for discovery of elusive and valuable transformations, particularly in functionalization of bioactive heterocycles. In order to fully harvest the potential of VLPC in the context of complex molecule synthesis, a thorough understanding of the elementary processes involved is crucial. This would enable more rational design of suitable reagents and catalysts, as well as prediction of activated C−H sites for functionalization. Such knowledge is essential when VLPC is to be employed in retrosynthetic analysis of complex molecules. Herein, we present a density functional theory (DFT) study of mechanistic details in the C−H functionalization of bioactive heterocycles exemplified by the methylation of the antifungal agent voriconazole. Moreover, we show that readily computed atomic charges can predict major site-selectivity in good agreement with experimental studies and thus be informative tools for the identification of active C−H functionalization sites in synthetic planning.

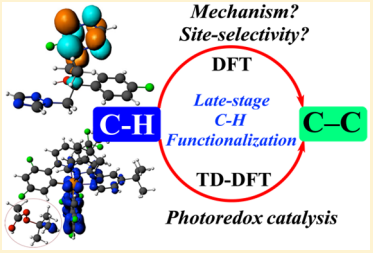

1. INTRODUCTION

Visible-light photoredox catalysis (VLPC) is emerging as a powerful approach to late-stage C−H functionalization.[1−7] Several examples of new reactions in this manifold have appeared in recent years in which unreactive C−H bonds have been converted into valuable C−C or C−X (X = N, O) bonds. Synthetic methods enabling structural diversification while avoiding prefunctionalization are powerful tools for medicinal chemists. Late-stage introduction of desired functional groups can allow fine-tuning of bioactive compounds to address common problems with bioavailability, activity, pharmacokinetics, and metabolism among others. Visible-light photoredox catalysis now has a demonstrated track-record of providing useful transformations to the medicinal chemistry toolkit.[8] Most notably, VLPC has been used in late-stage alkylation of biologically active heterocyles by DiRocco and co-workers.[9] The team described a general strategy for selective late-stage heterocycle alkylation of complex bioactive heterocycles based on photocatalytic activation of alkylperoxyacetates. A great example is the methylation of the antifungal agent voriconazole (Scheme 1), affording 75% yield of a 2.9:1 mixture of mono- and dimethylated product. Considering that voriconazole possesses ten distinct C−H sites and other functional groups, the result really highlights the potential of visible-light photocatalysis to effect highly regio- and chemoselective transformations.[9] A new era of sophisticated methodologies for synthesis is emerging through the photocatalytic reaction manifold,[3,7,9−15] and the need to develop a profound understanding of the underlying elementary processes is increasing.

Scheme 1. Late-Stage C−H Methylation Enables Structural Fine-Tuning to Address Problems in Medicinal Discovery and Development[9]

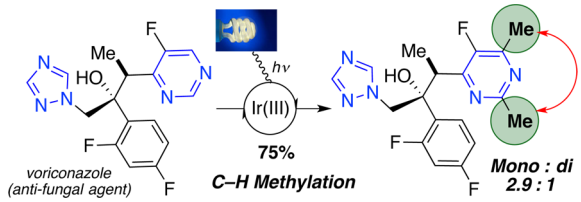

Radical-mediated C−H functionalization has become an important strategy to functionalize heterocyclic organic compounds,[7−9,16−18] particularly since selectivities are often complementary to those of other contemporary methods for directed C−H activation.[7−9,18] C−H bond functionalization in this context faces major challenges.[19] The first is concerning a thorough understanding of mechanisms, because this will be crucial for further developments in the field. The types of functionalization reagents amenable to photocatalytic activation will be important in defining the versatility of such methods. The second is related to site-selectivity in order to target functionalization of a single C−H bond. This is particularly important in complex molecules where distinction between multiple sites may not be obvious. The selective functionaliza-

Special Issue: Photocatalysis

Received: April 29, 2016
Published: June 27, 2016

DOI: 10.1021/acs.joc.6b00977
J. Org. Chem. 2016, 81, 7110−7120

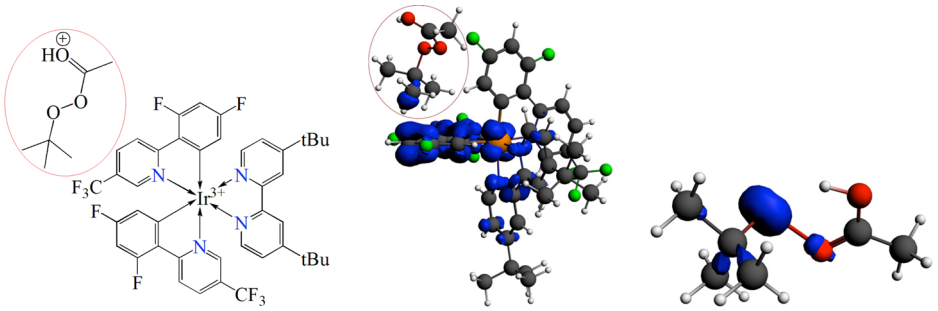

Figure 1. (left) Structure of the catalyst, $[Ir(dF\text{-}CF_3\text{-}ppy)_2(dtbpy)]^+$, and the radical source, *tert*-butylperoxyacetate; (middle) spin density plot (contour value of 0.03 au) showing the transfer of an electron from $[Ir(dF\text{-}CF_3\text{-}ppy)_2(dtbpy)]^+$ to the radical source (TBPA, in the circle) calculated using TD-B3LYP-D3BJ/LANL2TZ(6-311+G(d,p))/DMSO; (right) spin density plot (contour value of 0.01 au) for the separated TBPA after accepting an electron from the photocatalyst (note that the O−O bond is very elongated).

tion of a specific C−H bond is a fundamental problem and is, in many cases, extremely difficult.[20,21]

Density functional theory (DFT) enables a useful computational approach to assist design and interpretation of chemical experiments. In an earlier study, we have used DFT to calculate redox potentials of common and new photoredox catalysts.[22] We showed that DFT can be a powerful tool for prediction of redox properties, structure, and design of efficient catalysts, as well as for the potential identification of suitable catalyst−substrate combinations.[22,23] DFT can provide a detailed thermodynamic analysis as well as structural and kinetic information on the photocatalytic processes. Moreover, it can potentially be employed to identify active C−H sites in the functionalization step via readily computed parameters. Particularly in complex molecules, the electron distribution may not be clear enough by simple inspection for unambiguous determination of the preferred C−H site. DFT calculated parameters that could enable prediction would be useful for planning chemical synthetic transformations with VLPC C−H functionalization.

Since radicals can be either electrophilic or nucleophilic in nature, the prediction of such properties would be crucial in order to assess the reactive site of C−H functionalization in given complex molecules. Both electrophilicity and nucleophilicity indices can be predicted with DFT based on the highest occupied molecular orbital (HOMO) and lowest unoccupied molecular orbital (LUMO) energies.[24−27] Reasonable atomic charge descriptions can be predicted using the quantum theory of atoms in molecules (QTAIM)[28] and natural bond orbital (NBO)[29−31] analyses. In general, several approaches exist to assess reactivities, and it would be of great utility if a readily computed parameter could be employed.

In this paper, we have used state-of-the-art DFT calculations to analyze various aspects of visible-light photocatalytic C−H functionalization. A total of 62 molecules were considered, of which 8 are bioactive molecules. We also present a detailed analysis of the photocatalytic reaction mechanism for the methylation of voriconazole (a triazole antifungal drug)[32] as a model system for complex molecule C−H functionalization. We present computational evidence and details in favor of the established reaction mechanism. The addition of methyl radical to voriconazole has been studied in detail using relaxed potential energy surface scans of the reaction coordinates to clarify energetics involved in the processes and to identify the suitability of this approach as a tool for prediction. Moreover, we have computed the free energies along the relevant reaction pathways. Finally, we have attempted to establish simple predictors of site selectivity in VLPC C−H functionalization by comparing atomic charges and frontier orbitals. In this work, we demonstrate the utility of DFT calculations as a supplementary tool for synthetic planning with late-stage functionalization.

2. RESULTS AND DISCUSSION

2.1. Photocatalytic Activation. Versatile substrate structures amenable to activation are crucial to define the scope and limitations of photocatalyzed transformations for synthesis. An important property is the ability to engage in redox chemistry either directly with the excited-state photocatalyst or via another additive in the reaction mixture. A range of suitable redox-active moieties now exist for engaging in photoredox catalysis, including organic halides,[14] diazonium salts,[33] peroxides,[9] Michael acceptors, sulfamides, thiolates, alkenes, aryls, and heteroaryls and more.[1] In principle, given that our mechanistic knowledge is accurate, we should be able to predict suitable catalyst−precursor pairs that would react in the presence of light activation.

The mechanisms of activation depend strongly on the precursor structure. Precursors engineered with low-energy LUMOs can undergo single-electron reduction via a suitable photocatalyst, whereas systems with high-energy HOMOs can undergo single-electron oxidation. Electron-transfer can occur directly via a precursor complex with the catalyst or via another additive. We have previously shown how DFT can predict photocatalytic one-electron reduction of dimethyl bromomalonate leading to spontaneous extrusion of bromide ion and formation of the malonyl radical.[22] This occurs without any potential energy barrier. However, a contribution from the Marcus reorganization energy may be significant, but this is beyond the scope of this paper.[34]

The recent work of DiRocco and co-workers[9] demonstrates photocatalytic activation of alkylperoxyacetates through direct single-electron transfer from the excited-state photocatalyst. The process can produce nucleophilic alkyl radicals and proved to be a powerful late-stage functionalization tool for medicinal compounds.[8] We decided to visualize the protonated *tert*-butylperoxyacetate (TBPA) substrate in the vicinity of the photoredox catalyst $[Ir(dF\text{-}CF_3\text{-}ppy)_2(dtbpy)]^+$ ([4,4′-bis(1,1-dimethylethyl)-2,2′-bipyridine-*N*1,*N*1′]bis[3,5-difluoro-2-[5-(trifluoromethyl)-2-pyridinyl-*N*]phenyl-*C*]iridium(III), shown in Figure 1, left) in its excited state using time dependent (TD)-DFT calculations in order to support the proposed single-electron transfer. Figure 1 (middle) shows buildup of spin density on TBPA when in the vicinity of the photoexcited catalyst. This shows that the electron transfer process is

DOI: 10.1021/acs.joc.6b00977
J. Org. Chem. 2016, 81, 7110−7120

occurring in the precursor complex. The electron transfer is triggered by the difference in the redox potentials of the excited photocatalyst and the radical source; $E^{\circ}(Ir^{4+}/Ir^{3+*}) = -0.77$ V versus saturated calomel electrode (the experimental value is −0.89 V),[14] and 0.41 V for TBPA, both calculated using B3LYP-D3BJ/LANL2TZ(6-311+G(d,p))/DMSO. Moreover, it is known that alkyl peroxyactetates are electrocatalytically reducible.[35,36] When we visualize the spin-density plots of the optimized structure of TBPA after electron transfer, it clearly shows that the electron gained from the activated photocatalyst is localized at the oxygen atom attached to *tert*-butyl (Figure 1, right).

The described methylation reaction starts with excitation of the photocatalyst upon exposure to visible light. The photoactivated catalyst then transfers a single electron to the protonated TBPA followed by a C−C bond-breaking process for the formation of methyl radical (Figure 2a). Once TBPA

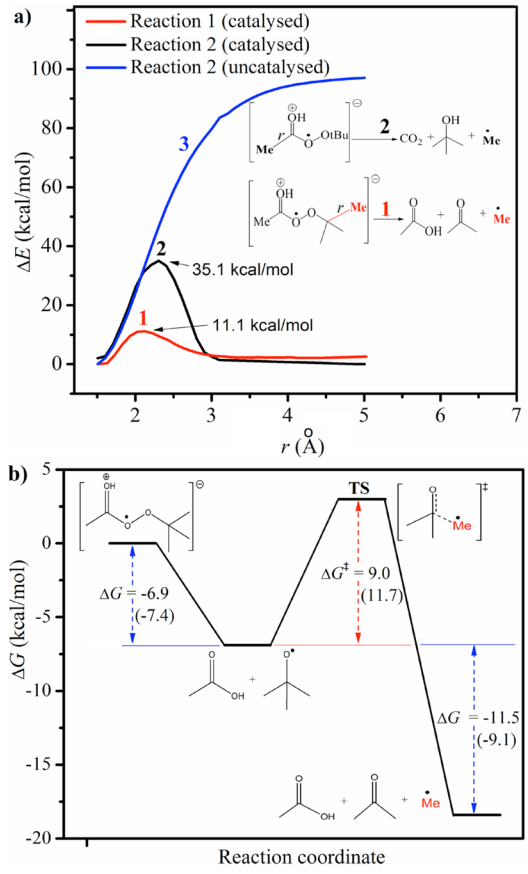

Figure 2. (a) PES diagram (ΔE versus r) for the generation of methyl radical from *tert*-butylperoxyacetate (TBPA) in the absence and presence of the photocatalyst (see Figures S1 and S2 of the SI for other examples); (b) Gibbs free energy diagram for reaction 1. The results without parentheses are calculated using uB3LYP-D3BJ/6-311+G(d,p)/DMSO and those in parentheses are calculated using uωB97XD/6-311+G(d,p)/DMSO.

gains an electron from the catalyst, there are in principle two possibilities to generate the methyl radical: one from the methyl attached to the carbonyl carbon (path 2) and the other from the *tert*-butyl substituent (path 1). When the activated photocatalyst supplies an electron to TBPA, the H_3C−C bond can easily break with a reasonably low activation energy barrier (see PES 1 and 2 of Figure 2a). Breaking the H_3C−C bond without the single-electron reduction is not a favored chemical process (see PES 3 of Figure 2a).

Generating methyl radical from the CH_3 attached to the carbonyl carbon displays a higher transition state barrier (35.1 kcal/mol), while that from *tert*-butyl has a lower energy barrier (11.1 kcal/mol), making the latter the feasible chemical process. Acetone and acetic acid are the only byproducts from the latter reaction, and this is in perfect agreement with the experimental observations.[9] Attempts to get the transition state structure for the concerted reaction mechanism were unsuccessful due to the defragmentation of the molecule upon the transition-state search. Additional calculations were performed by first scanning the O−O bond distance to form the *tert*-butoxy radical and acetic acid (Figure S1a of the Supporting Information (SI)) followed by scanning the C−C bond of the *tert*-butoxy radical from which the methyl radical is generated (Figure S1b of the SI). The former process is barrierless, whereas the latter has an energy barrier of 11.6 kcal/mol. This slight energy barrier difference compared with 11.1 kcal/mol (Figure 2a) seems to favor the concerted reaction mechanism in which the two byproducts are formed simultaneously with the radical formation step. On the other hand, the energy profile diagram in Figure 2b favors a stepwise defragmentation of the radical source to form acetic acid and *tert*-butoxy radical followed by the formation of acetone and methyl radical with a free energy barrier of 9.0 kcal/mol. To see the effect of protonation on the PES plots, we performed the scans with and without protonation of TBPA, and the results do not show considerable differences ($\Delta\Delta E$ = 0.5 kcal/mol). For a similar analysis of other photocatalytic activation processes to generate 4-pyridylmethyl, cyclopropyl, and malonyl radicals, see Figures S2 and S3 of the Supporting Information and ref 22, respectively.

We see that a DFT treatment of the activation process can predict the reaction pathway as well as refine our mechanistic understanding. This suggests that DFT can be employed in screening for potential new and effective substrates suitable for photocatalytic activation. We are currently working in this direction where DFT is guiding our experimental investigations into synthetically attractive functionalization agents.

2.2. Mechanistic Aspects of Radical C−H Functionalization. Subsequent to the photocatalytic activation step, a radical C−H functionalization process can occur on suitable C−H sites. As a case study for this process, we chose again the recently described late-stage alkyl functionalization of voriconazole (**1**). This is an interesting example, because it contains three aryl rings with different electronic environments, and it may not be straightforward to predict the site of preferred radical addition. Moreover, it would be of great interest to elicit energy barriers for the elementary reactions involved in the overall reaction to achieve a more complete understanding and enable rational design in the future.

From experimental studies, we know that the pyrimidine ring contains the preferred sites of attack. However, charge calculations using NBO and QTAIM atomic charges suggested that the carbon atoms of the triazole ring are significantly positive as well (for instance, the QTAIM charges are +0.940 and +0.954 for the two carbon atoms, (*vide infra*)). We decided to investigate whether simple relaxed coordinate scans of methyl radical approaching various sites in the molecules would reveal (1) the preferred site of addition and (2) the magnitude of energy barriers in this type of addition. The potential energy surfaces for methyl radical addition to sites Ca−Cb can be seen

DOI: 10.1021/acs.joc.6b00977
J. Org. Chem. 2016, 81, 7110−7120

in Figure 3a. All barriers are relatively low (<10 kcal/mol). The analysis does predict the lowest barrier of 6.7 kcal/mol for the

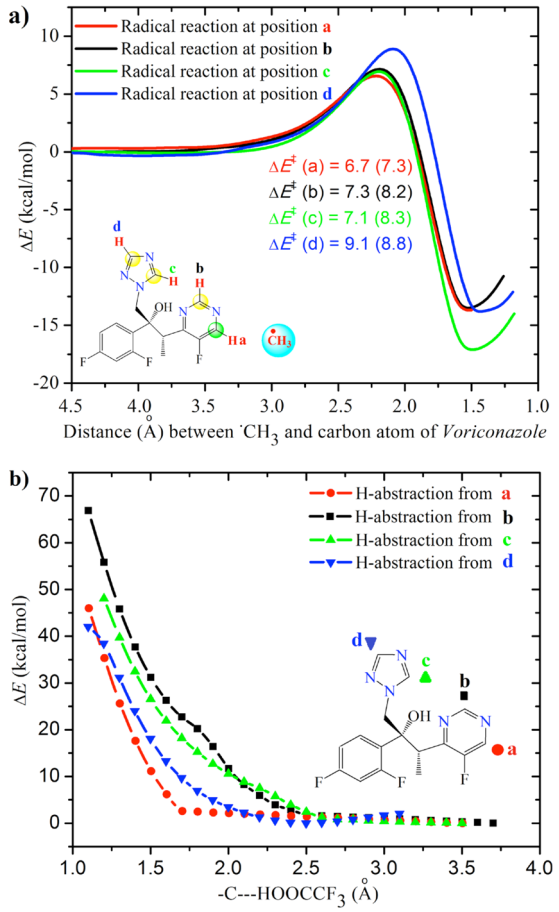

Figure 3. (a) PES for the different possible reactions between methyl radical and voriconazole to form methylated radical intermediate products. $\Delta E^{\ddagger}$(TS) without parentheses are calculated using uB3LYP-D3BJ/6-311+G(d,p)/DMSO and those in parentheses are calculated using uωB97XD/6-311+G(d,p)/DMSO. (b) PES for proton abstraction from the methylated intermediate product by TFA^{-}. Note that this last reaction follows the single electron transfer from the radical intermediate products to the oxidized catalyst generated during the methyl radical formation.

experimentally determined site of preferred addition; however, the other barriers are marginally larger and do not reflect the experimental observations of methylation only at positions a and b.[9] This demonstrates that care must be taken when performing such a PES analysis and that it may not be the sole and suitable approach to determine site selectivity.

Subsequent to radical addition, an oxidation of the adduct must occur to generate the corresponding cationic species suitable for proton elimination to generate the C−H functionalized product. We will discuss the oxidation below but also investigated here whether deprotonation of the cationic intermediate could be effected by trifluoroacetate anion (TFA^{-}). Figure 3b shows the PES for proton abstractions by TFA^{-} in the four cases mentioned above (a−b), which all reveal that a highly favored, barrierless proton elimination is feasible.

A detailed photocatalytic reaction mechanism is presented in Figure 4 (for the Ca and Cb radical additions; and in Figure S4 of the SI for positions Cc and Cd) where the calculated change in reaction energies and transition state energy barriers for all the processes are summarized. This reveals that the photocatalytic activation step barrier is similar or smaller than the radical addition barriers. Barriers for electron transfer steps still remain elusive and are beyond the scope of this paper. This would involve the additional complexity of estimating the reorganization energy from Marcus theory[34] and will be considered in future work. The B3LYP-D3BJ calculated free energy barrier $\Delta G^{\ddagger}$ for the Ca and Cb radical additions are 14.9 and 16.8 kcal/mol, respectively, which indicate that the Ca addition is favored. The results obtained from ωB97XD calculations also reproduce these trends (Figure 5).

The proposed single-electron oxidation by the oxidized photocatalyst displays a favorable thermodynamic driving force (note also that the B3LYP-D3BJ/LANL2TZ(6-311+G(d,p))/DMSO calculated $E^{\circ}(Ir^{4+}/Ir^{3+})$ is 1.39 V and that of voriconazole is −2.12 V, both versus SCE). All four sites investigated are comparably exoergic by about 6−14 kcal/mol. The overall reaction is strongly exoergic at −80.4 kcal/mol for reaction at the preferred Ca site. Transition state calculations and PES scans indicate that formation of the bismethylated adduct from the Cb-monomethylated product has a barrier of 6.49 kcal/mol, and slightly higher 7.72 kcal/mol (see Figures S5 and S6 of the SI) when starting from the Ca-monomethylated product. This indicates that the observed dimethylation product is formed by a second methylation of the Cb-methylation product. This is consistent with the experimental observation of only monomethylation product at Ca.

Transition state searches were performed using the quadratic synchronous transit approach (QST3)[37,38] and Gibbs free energies were calculated along the reaction coordinate. The results are presented in Figure 5 and Figure S7 of the SI. The study supports that radical methylation at site Ca is more favored with a free energy barrier of 14.9 kcal/mol versus 16.8 kcal/mol for addition at Cb. Further analysis of the free energies shows that the radical addition steps have similar exergonicity (−2.8 and −1.9 kcal/mol for Ca and Cb additions, respectively) and that the reaction proceeds downhill to the expected products upon formation of the radical intermediate. The photocatalyst oxidation step is exergonic by −10.7 kcal/mol for Ca-addition, followed by barrierless deprotonation to afford an overall exergonicity of −84.7 kcal/mol (from the radical intermediate).

In order to obtain a more general idea of the magnitude of free energy changes and barriers for other radical additions with the alkylperoxyacetate system, we calculated Gibbs free energies of the reactions ($\sum G$(products) − $\sum G$(reactants)), change in entropies ($\sum S$(products) − $\sum S$(reactants)), and the free energy barriers of the transition states for the radical addition reactions for a selection of compounds with experimental data accessible (Figure 6). The free energy barriers range from about 12 to 17 kcal/mol, and the reactions are generally highly exergonic by 82−87 kcal/mol. We see that radical addition free energy barriers are quite similar to the photocatalytic activation step itself. Likely, there is a fine balance that must be achieved for a working system in this chemistry, because if the photocatalytic radical generation becomes faster than subsequent functionalization, a buildup of excess radical concentration could lead to more indiscriminate C−H functionalization. Control of selectivity is kinetically supported by low radical concentrations. At least in the case of alkyl peroxyacetates, since the free energy barriers of photocatalytic activation and radical addition are of similar magnitudes, this

DOI: 10.1021/acs.joc.6b00977
J. Org. Chem. 2016, 81, 7110−7120

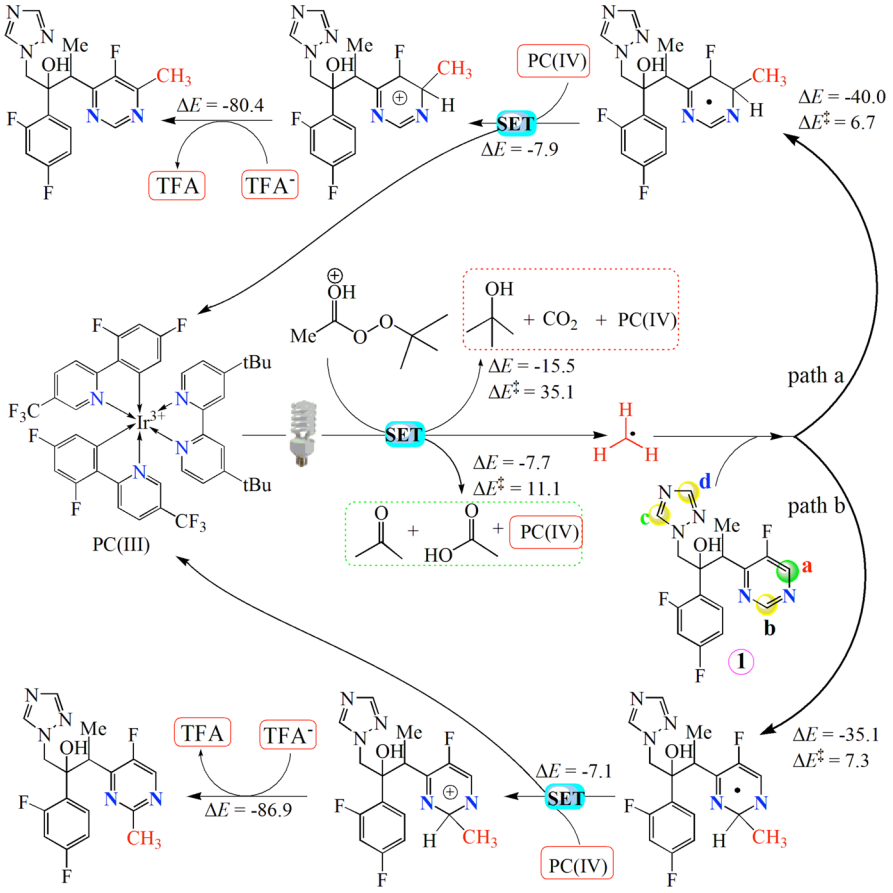

Figure 4. Reaction mechanism for the photocatalytic C−H functionalization of voriconazole showing different potentially competing reactions (paths a and b, see Figure S4 of the SI for paths c and d). ΔE (kcal/mol) are calculated using TD-B3LYP-D3BJ/6-311+G(d,p)/DMSO in the excited state. $\Delta E^{\ddagger}$ values are obtained from the PES scans performed in the ground state and presented in Figure 3a (see Figure 5 for $\Delta G^{\ddagger}$ values). SET stands for single-electron transfer. TFA was considered as a proton donor to the radical source and TFA^{-} as a hydrogen abstractor in the final reaction steps and regenerating TFA.

suggests that selectivity is maintained by the low concentration of the photoexcited catalyst.

The use of global reactivity indexes like electronic chemical potential (μ), chemical hardness (η), global electrophilicity index (ω), and global nucleophilicity index (N) could assist prediction of the overall reactivity of the molecules. In cases where the electronic nature of the radical is not clear, for example, in captodative radicals, these indexes can identify whether they act as nucleophiles or electrophiles with a given complex molecule. For instance, the calculated natural charges from the NBO analysis on the carbon atoms of CF_3 (global electrophilicity index (ω) of 3.236 eV and global nucleophilicity index (N) of 1.251 eV) and CH_3 (ω = 2.226 eV, N = 2.606 eV) radicals are 1.025 and −0.484, respectively; whereas the total atomic charges are 0.313 and −0.452, respectively. These results quantitatively indicate that the former is an electrophile while the latter is a nucleophile. However, this may be more useful for cases where simple inspection is not straightforward and should be used with care.[39]

In this section, we have demonstrated that DFT can be employed in explicitly studying radical additions in detail, and the results gave a qualitatively correct prediction of the preferred site of attack. The similarity between the calculated potential energy barriers demonstrate that site differentiation is finely balanced in this chemistry and that DFT is struggling to clearly distinguish between sites in this analysis. This is clearly supported by the observation of dimethylation in the experimental work by DiRocco and co-workers.[9] The use of potential energy surface scans with constrained reaction coordinates can lead to confusing results, because the calculated barriers would predict addition also to the triazole unit. However, it is important to consider that this represents a constrained analysis and does not necessarily reflect the full reality of the system. The predicted energy changes in the C−H methylation of voriconazole indicate a mechanism consisting of radical addition followed by oxidation to cation and a barrierless proton elimination by trifluoroacetate anion. These studies suggest that visible-light photocatalyzed C−H alkylations work well due to the slow formation of radicals (controlled by a low concentration of the excited-state catalyst) with subsequent rapid addition, oxidation, and elimination to form the observed products.

2.3. Site-Selectivity in Heterocycle Functionalization.

The prediction of preferred site of functionalization would be of great interest to the chemical community if photocatalytic methods are to be used strategically in synthetic planning. This becomes more important with increasing molecular complexity, because the preferred site of attack may be less clear. We set out to investigate whether DFT could provide easily calculated parameters that would enable rapid prediction of site selectivity. A recent experimental study of radical site selectivity by Baran and co-workers described a range of substituted heterocycles

DOI: 10.1021/acs.joc.6b00977
J. Org. Chem. 2016, 81, 7110−7120

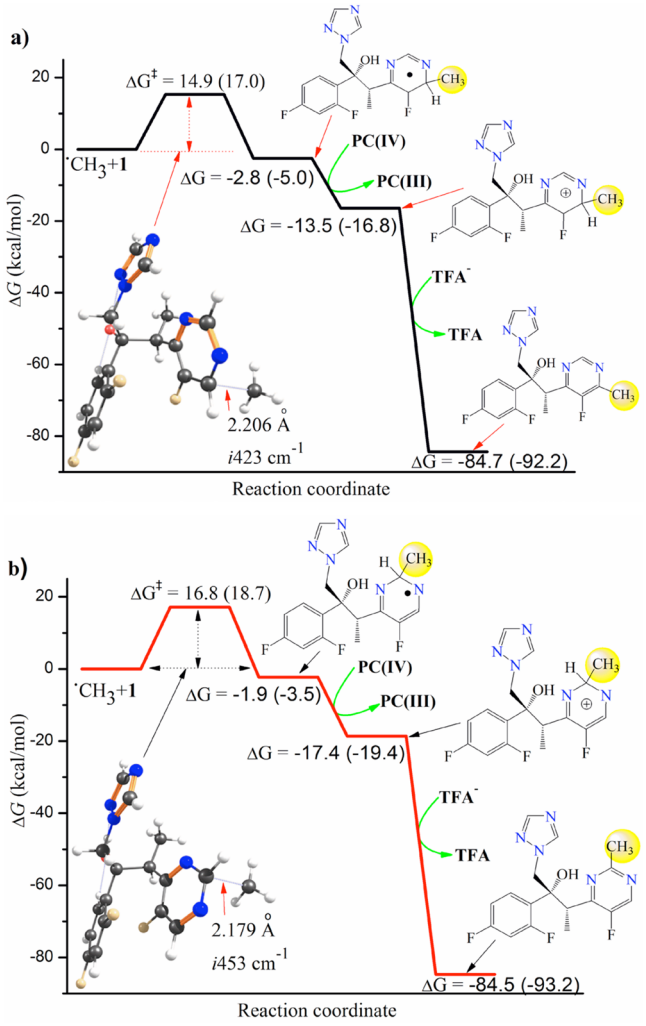

Figure 5. Gibbs free energy diagram for methylation of voriconazole: (a) Ca methylation; (b) Cb methylation. Change in Gibbs free energies (in kcal/mol) without parentheses are obtained using B3LYP-D3BJ/6-311+G(d,p)/DMSO, whereas those in parentheses are obtained using ωB97XD/6-311+G(d,p)/DMSO. The inset structures are transition state geometries together with the C···C bond lengths and the corresponding imaginary frequencies. Transition state free energy barriers are obtained using the QST3 approach.

that they employed to develop predictive rules.[18] If the preferred sites of C−H functionalization could be efficiently predicted by DFT, this could alleviate exhaustive experimental studies and extensive predictive rules of this kind and enable efficient and accurate synthetic planning with complex molecules. Moreover, variability in functional groups and their positions could be effectively probed. Furthermore, the optimized structures would enable analysis of steric effects that could override intrinsic electronic preferences.

One of the simplest parameters available is charge. Atomic charges could potentially reveal the most electrophilic sites and hence predict sites of attack by nucleophilic radicals and vice versa. This would be a straightforward parameter to compute and, thus, be a powerful predictive tool for synthetic planning. We decided to investigate a range of heterocycles (a total of 62 molecules), some of which were described in the recent study by Baran.[18] The 62 structures studied herein, together with their natural bond orbital (NBO) and quantum theory of atoms in molecules (QTAIM) atomic charges are presented in Figure 7 for **1**−**4**, Figure 8 for **5**−**8**, and Figure 9 for **9**−**17**; whereas **18**−**62** are presented in the Supporting Information (Figures S8−S12). The reactions are not all photocatalytic; we have also included reactions where radical intermediates are generated and subsequently added to heterocyclic systems. Since the photocatalyzed reactions can be conducted in acidic medium, the heteroatoms could be protonated and thus modulate the charge distribution. Hence, additional calculations were performed for protonated molecules (Figure S13 of the SI). Calculations were also performed in the excited state for the protonated molecules (Figure S14 of the SI) in order to investigate any charge redistribution effects.

We set out to determine whether atomic charge could be a reliable predictor of site selectivity, since positive charge would make carbon atoms more susceptible to nucleophilic radical attacks. However, there are problems with interpreting the absolute meaning of the numerical value of calculated charges, and we therefore computed both NBO and QTAIM charges for comparison and interpreted the numbers with caution. In most of the 62 molecules studied, one specific carbon site (highlighted in green) had the most positive NBO and QTAIM charges. In some of the molecules, there are secondary carbon atoms expected to be competing sites based on similar numerical charge values. For instance, in **1**, **9**, **10**, **20**, and **22**, two carbon atoms are predicted to have positive charges.

The overall results show that the predicted activated sites based on atomic charges are in generally good agreement with the corresponding experimentally determined products (compare yields in red circles and the green-highlighted carbon atoms in Figures 7−9). It is difficult to differentiate between methods, because NBO and QTAIM charges interchangeably give the best prediction. Looking at more complex, bioactive molecules, **2** and **5** (Figures 7 and 8) show very good correlations with charge calculations. In **7**, the predicted site of nucleophilic addition is indicated; however, the experimental result involves addition of the trifluoromethyl radical acting as an electrophilic radical at a nucleophilic C−H-site in this case. We predicted C2 functionalization for **6** (Figure 8); however, a C5 functionalized product is reported in ref 18, where the authors stated that this unusual product is under investigation. The computed global electrophilicity and nucleophilicity indices for **7** support that this is likely to react as a nucleophile. In voriconazole **1**, the observed sites of functionalization are predicted, but charges also predict possible addition to the triazole ring. For simpler π-deficient heterocycles **9**−**23**, the predictions are generally good, but charges cannot be used to determine major or minor sites in cases with multiple additions. Clearly, simple predictions based solely on atomic charges can have limitations as shown in these examples. However, the most positively charged carbon atom provides a good estimate of preferred functionalization site.

The presence of an acid in the reaction medium may affect the charge distribution. Experimental findings also confirm that protonating pyridines can enhance their reactivity.[40,41] In Figure S13 of the SI, it is shown that some carbon atoms get more positive charges while others get more negative charges upon protonation. Test calculations were also performed in the excited state. However, excitation of the molecules does not affect considerable change in the atomic charges of the active sites, even though some charge gains are observed on a few carbon atoms (Figure S14 of the SI).

The use of computed QTAIM and NBO charges as simple predictors for potential reactive C−H sites should be of

DOI: 10.1021/acs.joc.6b00977
J. Org. Chem. 2016, 81, 7110−7120

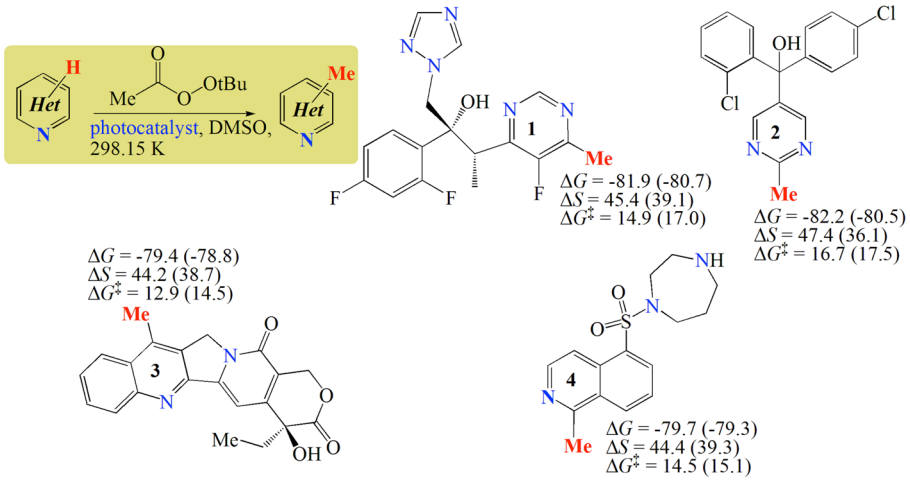

Figure 6. Change in Gibbs free energies (ΔG, in kcal/mol) and change in entropies (ΔS, in cal/(mol·K)) for the formation of the C−H functionalized molecules **1**−**4** (based on only the reactants and the final products). The results without parentheses are obtained using B3LYP-D3BJ/6-311+G(d,p)/DMSO, whereas those in parentheses are obtained using ωB97XD/6-311+G(d,p)/DMSO. Transition state free energy barriers ($\Delta G^{\ddagger}$, in kcal/mol) for the radical additions are calculated using the QST3 approach.

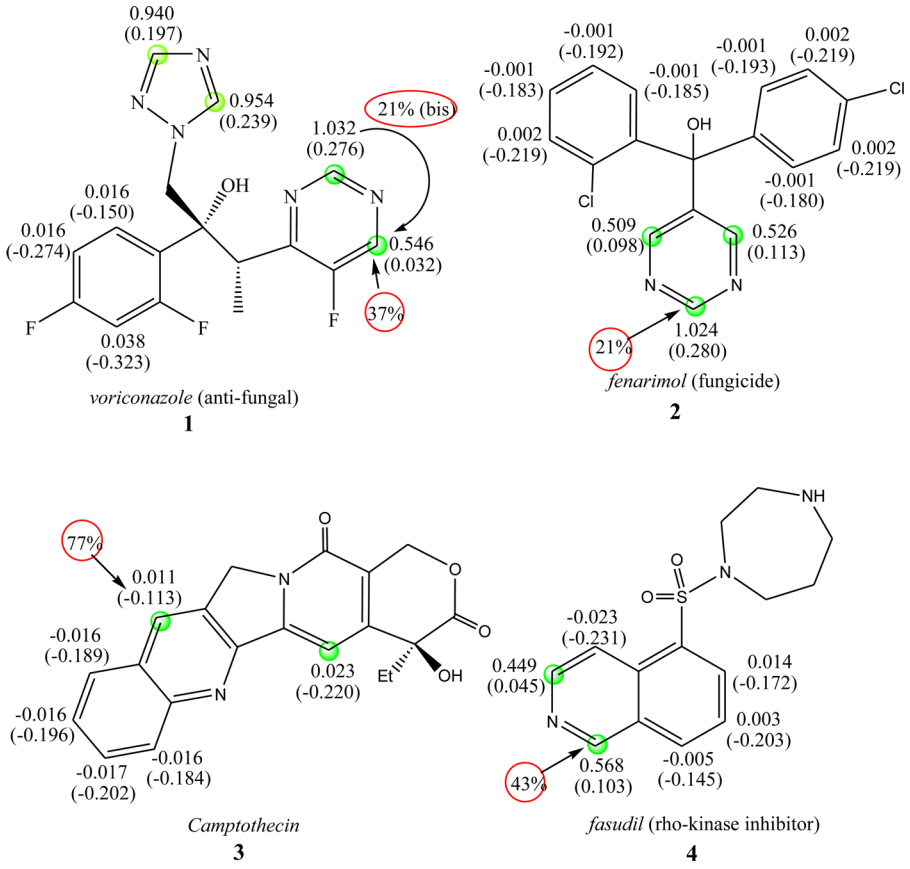

Figure 7. Radical site selectivity of **1**−**4**. The green circles highlight positions that are susceptible for radical attack. The numbers without parentheses are atomic charges obtained from QTAIM calculations, while those in parentheses are natural charges from NBO analysis, both calculated using B3LYP-D3BJ/6-311+G(d,p)/PCM/DMSO calculations. The numbers given in the red circles are percentage yields from experiments; **1**, **3**, and **4** from ref 9, **2** from ref 18. Radicals used: CH_3 for **1**, **3** and **4**, and isopropyl (*i*-Pr) for **2**.

significant importance for synthetic planning with photocatalytic C−H functionalization, simply by identifying the positively charged sites (susceptible for nucleophilic radical addition). In Figures 7 and 8, a number of biologically active heterocyclic molecules are listed together with their NBO and QTAIM atomic charges. The presence of more than one aromatic ring makes it increasingly difficult to identify the activated sites for the radical attack. The calculated charges allow for prediction of potential sites.[9] In some cases, such as voriconazole **1**, prediction based solely on charge may be confusing. Here, the triazole unit has significantly positively charged carbons (+0.9), which may lead to the false prediction

DOI: 10.1021/acs.joc.6b00977
J. Org. Chem. 2016, 81, 7110−7120

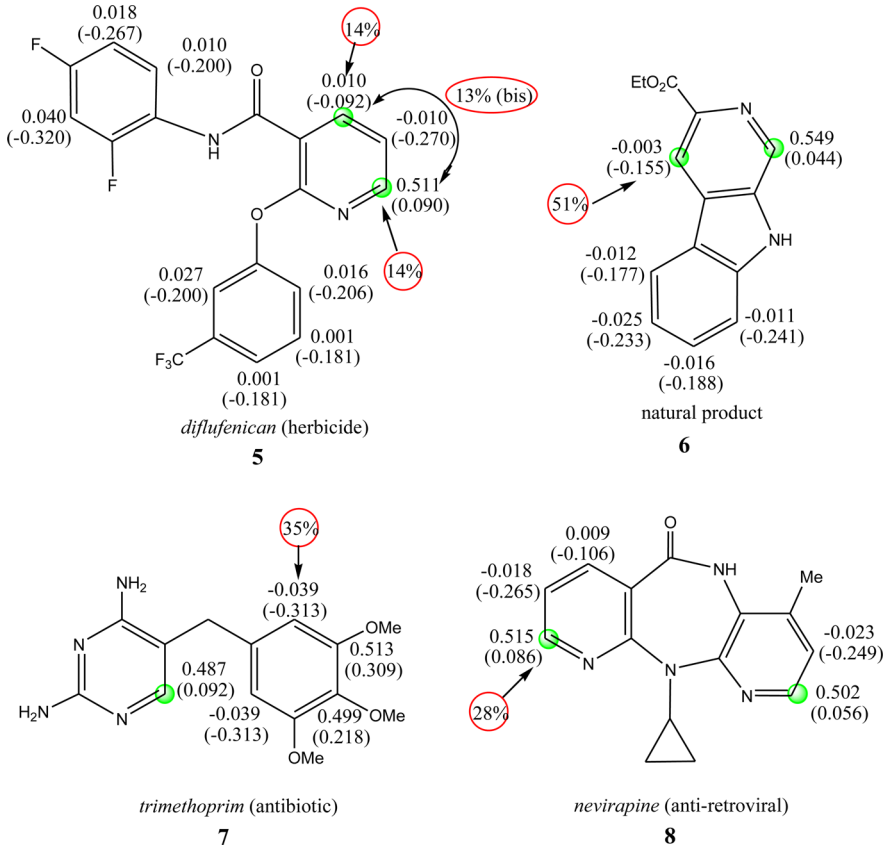

Figure 8. Radical site selectivity of **5**–**8**. The green circles highlight positions that are susceptible for radical attack. The numbers without parentheses are atomic charges obtained from QTAIM calculations, while those in parentheses are natural charges from NBO analysis, both calculated using B3LYP-D3BJ/6-311+G(d,p)/PCM/DMSO calculations. The numbers given in the red circles are percentage yields from experiments; **5** from ref 9, **6**–**8** from ref 18. Radicals used: CH_3 for **5**, CF_3 for **7**, *i*-Pr for **6** and **8**.

of active C–H sites. A slightly more refined analysis is now necessary for accurate prediction.

When atomic charges proved inconclusive or confusing for prediction of active C–H sites we decided to visualize the Kohn–Sham frontier orbitals of the system in order to shed more light on the selectivity (Figure 10). In the case of voriconazole, the LUMO is clearly localized on the pyrimidine ring system and the orbital plot demonstrates the magnitude of the LUMO density to be largest on the observed site of C–H functionalization (Ca). The reaction is controlled by frontier orbital interactions. KS-LUMOs for several molecules are further shown in the Supporting Information, and these plots enable a more refined prediction of the intrinsically activated sites for C–H functionalization in addition to the atomic charges.

In summary, the active sites susceptible for C–H functionalization can be reasonably predicted based on the charges obtained either from NBO analysis or QTAIM calculations. For single heterocyclic compounds, it may be possible to identify the active sites by simple inspection. However, this becomes increasingly complicated for more complex molecules with multiple heterocyclic units (see molecules **1**–**8**). However, when using these two approaches one has to consider the experimental conditions and the nature of the radicals. For instance, π-conjugation of substituents on the heterocycles may lead to a shift of reactive sites from what would be predicted in the parent heterocycle.[42,43] Protecting groups and steric effects are also important factors to be carefully considered in conjunction with the electronic analysis presented herein for synthetic planning. For instance, three reactive sites for possible nucleophilic radical addition are predicted for **2**, but the two ortho-sites are more sterically congested.

3. CONCLUSIONS

In this study, we investigated a total of 62 heteroaromatic organic molecules, of which 8 are drug-like molecules, with the aim of obtaining a quantitative understanding of the underlying mechanism and establish tools for the identification of site-selectivity in visible-light photocatalytic late-stage C–H functionalization. TD-DFT calculations indicate that radical generation from alkylperoxyacetates via photocatalysis occurs through single electron transfer directly from the photo-activated catalyst. Readily computed atomic charges from NBO analysis and QTAIM calculations are found to be useful parameters for identifying potential major active C–H functionalization sites. Refined predictions can be made by visualization of frontier orbitals and identification of sites with the largest contributions to these. Our results demonstrate how DFT can be employed to obtain quantitative and qualitative details on the reaction mechanisms of photocatalyzed transformations and provide a refined understanding of the elementary processes involved. Moreover, we have demonstrated that relatively straightforward calculations of atomic charges and frontier orbital visualizations enable prediction of site selectivity in radical additions to heterocycles. The ease at which state-of-the-art calculations can currently be made at

DOI: 10.1021/acs.joc.6b00977
J. Org. Chem. 2016, 81, 7110–7120

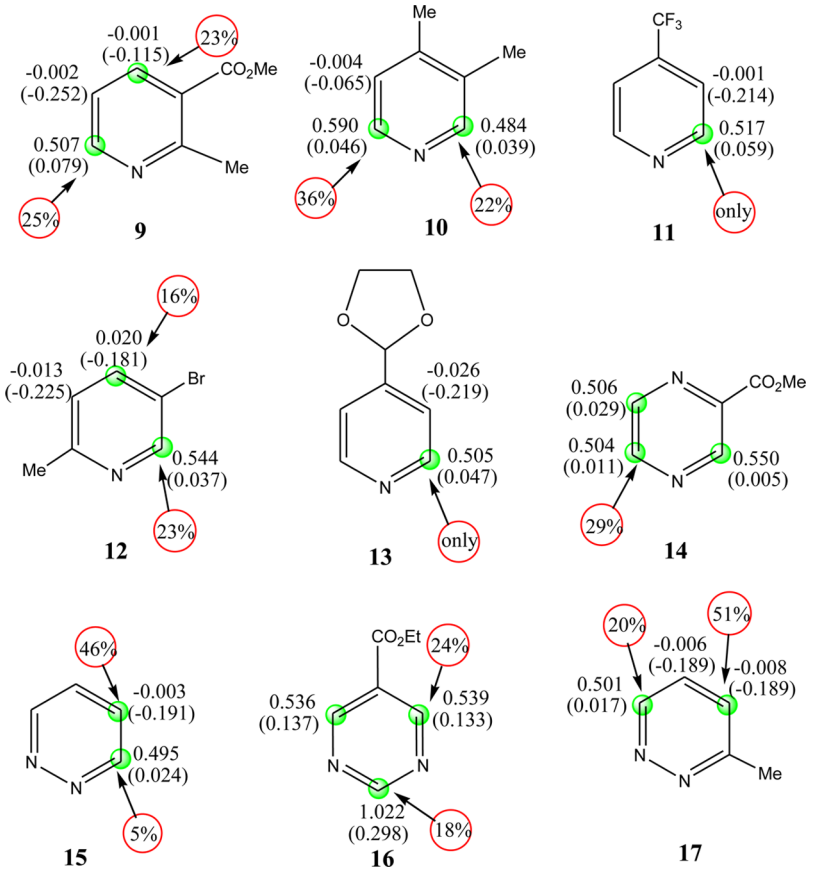

Figure 9. Radical site selectivity of simple substituted pyridines **9**–**17**. The green highlighted positions are predicted susceptible for nucleophilic radical attack. The numbers without parentheses are atomic charges obtained from QTAIM calculations, while those in parentheses are natural charges from NBO analysis, both calculated using B3LYP-D3BJ/6-311+G(d,p)/PCM/DMSO calculations. The numbers given in red circles are percentage yields from ref 18. Radicals used: CF_3 for **9**, **10**, and **12**; *p*-MeC_6H_4 for **11** and **13**; *i*-Pr for **14**–**17**.

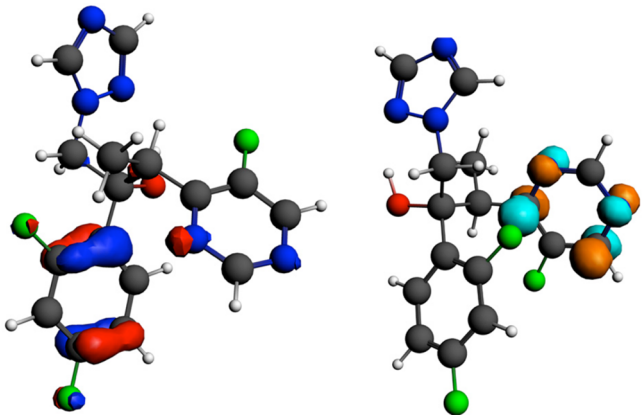

Figure 10. (left) Highest occupied molecular orbital (HOMO) and (right) lowest unoccupied molecular orbital (LUMO) of voriconazole (**1**) calculated using TD-B3LYP-D3BJ/6-311+G(d,p)/DMSO. A contour value of 0.06 au was used to plot the orbitals.

incredible speeds makes DFT a valuable tool for planning contemporary complex molecule synthesis with late-stage C–H functionalization.

4. COMPUTATIONAL DETAILS

All the DFT calculations were performed using the Gaussian 09[44] program package. The B3LYP[45−47] functional together with Grimme's dispersion correction[48] and Becke-Johnson damping corrections[49] (abbreviated as B3LYP-D3BJ) was used to account for the energetics of bond breaking and forming reaction steps. It has also been shown that this functional gives reasonable results for similar radical based studies.[23,39,50−53] Additional calculations for the reaction mechanisms were performed using the ωB97XD[54] functional which has also been shown to give satisfactory results.[55−58] For the light atoms the 6-311+G(d,p) basis sets[59] were used, whereas LANL2TZ effective core potential basis set[60] was used for the iridium atom of the photocatalyst to account for relativistic effects. The former basis sets have been used for such kind of studies.[40,51,52] The results from the two functionals are in close agreement with each other (*vide supra*), hence only the results from the B3LYP-D3BJ are cited in the results and discussions section. Solvent effects were corrected by using the polarizable continuum model (PCM) in its integral equation formalism[61] together with dimethyl sulfoxide (DMSO) as a solvent.

Conformational analyses for the structures of the nonrigid drug-like molecules were performed using the program packages Marvin view version 16.2.29.0 (http://www.chemaxon.com) and PCMODEL version 9.0 (http://www.serenasoft.com). The reactants as well as products have been assessed based on the potential energy surfaces (PESs) and the most stable geometry at the PES were considered for further calculations. The screened structures were further optimized using B3LYP-D3BJ/6-311+G(d,p). Vibrational frequency analyses were performed to verify that the optimized structures are minima without an imaginary frequency and to obtain the

DOI: 10.1021/acs.joc.6b00977
J. Org. Chem. 2016, 81, 7110−7120

thermal energy contributions to the free energies of the molecules. The transition state structures for the radical addition reactions were calculated using the quadratic synchronous transit approach (QST3)[37,38] in Gaussian 09 program package,[44] and were verified by the presence of only one appropriate imaginary frequency. For all the open-shell (radical) molecules as well as calculations involving bond-breaking and bond-forming steps, the unrestricted DFT approach was used, whereas the restricted approach was used in all the closed-shell calculations.

The NBO analysis[29−31] and the QTAIM[28] calculations were used to explore the charges on the atoms before and after the formation of new bonds during the chemical reactions, all obtained from the B3LYP-D3BJ/6-311+G(d,p) calculations performed in DMSO. It is important to note that the NBO charges were obtained from the direct geometry optimization steps using the pop=nbo keyword, whereas the QTAIM charges were calculated from the B3LYP-D3BJ/6-311+G(d,p) output using the AIMAll software[62] version 16.01.09. The electronic chemical potential (μ), chemical hardness (η), global electrophilicity index (ω) and global nucleophilicity index (N) were calculated based on the equations[24−27,39,63] described in the Supporting Information. The redox potentials are calculated based on the approaches described in ref.[22] For the sake of uniformity, all these analyses were also performed in DMSO.

■ ASSOCIATED CONTENT

Supporting Information

The Supporting Information is available free of charge on the ACS Publications website at DOI: 10.1021/acs.joc.6b00977.

Full citation of ref 44, computational details and explanations, charges for the molecules not shown in the main article, and frontier molecular orbitals (PDF)

The optimized geometries of the reactants, products, and transition state structures (XYZ)

■ AUTHOR INFORMATION

Corresponding Author

*E-mail: jorn.h.hansen@uit.no

Notes

The authors declare no competing financial interest.

■ ACKNOWLEDGMENTS

This work has received support from the Research Council of Norway [Grant Number 179568/V30] and the Department of Chemistry at UiT The Arctic University of Norway. Computer time was provided by the Norwegian supercomputing program NOTUR [Grant Number NN4654K].

■ REFERENCES

(1) Hoffmann, N. *Chem. Rev.* **2008**, *108*, 1052−1103.
(2) Fagnoni, M.; Dondi, D.; Ravelli, D.; Albini, A. *Chem. Rev.* **2007**, *107*, 2725−2756.
(3) Xuan, J.; Xiao, W.-J. *Angew. Chem., Int. Ed.* **2012**, *51*, 6828−6838.
(4) Wang, C.; Qin, J.; Shen, X.; Riedel, R.; Harms, K.; Meggers, E. *Angew. Chem., Int. Ed.* **2016**, *55*, 685−688.
(5) Peña-López, M.; Rosas-Hernández, A.; Beller, M. *Angew. Chem., Int. Ed.* **2015**, *54*, 5006−5008.
(6) Huo, H.; Wang, C.; Harms, K.; Meggers, E. *J. Am. Chem. Soc.* **2015**, *137*, 9551−9554.
(7) Cherevatskaya, M.; Neumann, M.; Füldner, S.; Harlander, C.; Kümmel, S.; Dankesreiter, S.; Pfitzner, A.; Zeitler, K.; König, B. *Angew. Chem., Int. Ed.* **2012**, *51*, 4062−4066.
(8) Cernak, T.; Dykstra, K. D.; Tyagarajan, S.; Vachal, P.; Krska, S. W. *Chem. Soc. Rev.* **2016**, *45*, 546−576.
(9) DiRocco, D. A.; Dykstra, K.; Krska, S.; Vachal, P.; Conway, D. V.; Tudge, M. *Angew. Chem., Int. Ed.* **2014**, *53*, 4802−4806.
(10) Gutekunst, W. R.; Baran, P. S. *Chem. Soc. Rev.* **2011**, *40*, 1976−1991.
(11) McMurray, L.; O'Hara, F.; Gaunt, M. J. *Chem. Soc. Rev.* **2011**, *40*, 1885−1898.
(12) Yamaguchi, J.; Yamaguchi, A. D.; Itami, K. *Angew. Chem., Int. Ed.* **2012**, *51*, 8960−9009.
(13) Furst, L.; Matsuura, B. S.; Narayanam, J. M. R.; Tucker, J. W.; Stephenson, C. R. J. *Org. Lett.* **2010**, *12*, 3104−3107.
(14) Nguyen, J. D.; D'Amato, E. M.; Narayanam, J. M. R.; Stephenson, C. R. J. *Nat. Chem.* **2012**, *4*, 854−859.
(15) Tucker, J. W.; Zhang, Y.; Jamison, T. F.; Stephenson, C. R. J. *Angew. Chem., Int. Ed.* **2012**, *51*, 4144−4147.
(16) Liu, D.; Li, Y.; Qi, X.; Liu, C.; Lan, Y.; Lei, A. *Org. Lett.* **2015**, *17*, 998−1001.
(17) Tang, S.; Liu, K.; Long, Y.; Qi, X.; Lan, Y.; Lei, A. *Chem. Commun.* **2015**, *51*, 8769−8772.
(18) O'Hara, F.; Blackmond, D. G.; Baran, P. S. *J. Am. Chem. Soc.* **2013**, *135*, 12122−12134.
(19) Demissie, T. B.; Hansen, J. H. *Dalton Trans.* **2016**, *45*, 10878−10882.
(20) Labinger, J. A.; Bercaw, J. E. *Nature* **2002**, *417*, 507−514.
(21) Bergman, R. G. *Nature* **2007**, *446*, 391−393.
(22) Demissie, T. B.; Ruud, K.; Hansen, J. H. *Organometallics* **2015**, *34*, 4218−4228.
(23) Gutierrez, O.; Tellis, J. C.; Primer, D. N.; Molander, G. A.; Kozlowski, M. C. *J. Am. Chem. Soc.* **2015**, *137*, 4896−4899.
(24) Domingo, L. R.; Chamorro, E.; Pérez, P. *J. Org. Chem.* **2008**, *73*, 4615−4624.
(25) Parr, R. G.; Donnelly, R. A.; Levy, M.; Palke, W. E. *J. Chem. Phys.* **1978**, *68*, 3801−3807.
(26) Parr, R. G.; Pearson, R. G. *J. Am. Chem. Soc.* **1983**, *105*, 7512−7516.
(27) Parr, R. G.; Szentpály, L. v.; Liu, S. *J. Am. Chem. Soc.* **1999**, *121*, 1922−1924.
(28) Bader, R. F. W. *Atoms in Molecules - A Quantum Theory*; Oxford University Press: Oxford, 1994.
(29) Weinhold, F.; Landis, C. R. *Chem. Educ. Res. Pract.* **2001**, *2*, 91−104.
(30) Weinhold, F.; Landis, C. R. *Discovering Chemistry With Natural Bond Orbitals*; John Wiley & Sons: Hoboken, NJ, 2012.
(31) Reed, A. E.; Curtiss, L. A.; Weinhold, F. *Chem. Rev.* **1988**, *88*, 899−926.
(32) Herbrecht, R.; Denning, D. W.; Patterson, T. F.; Bennett, J. E.; Greene, R. E.; Oestmann, J.-W.; Kern, W. V.; Marr, K. A.; Ribaud, P.; Lortholary, O.; Sylvester, R.; Rubin, R. H.; Wingard, J. R.; Stark, P.; Durand, C.; Caillot, D.; Thiel, E.; Chandrasekar, P. H.; Hodges, M. R.; Schlamm, H. T.; Troke, P. F.; de Pauw, B. *N. Engl. J. Med.* **2002**, *347*, 408−415.
(33) Hari, D. P.; Schroll, P.; König, B. *J. Am. Chem. Soc.* **2012**, *134*, 2958−2961.
(34) Ren, H.-S.; Ming, M.-J.; Ma, J.-Y.; Li, X.-Y. *J. Phys. Chem. A* **2013**, *117*, 8017−8025.
(35) Baron, R.; Darchen, A.; Hauchard, D. *Electrochim. Acta* **2006**, *51*, 1336−1341.
(36) Baron, R.; Darchen, A.; Hauchard, D. *Electrochim. Acta* **2004**, *49*, 4841−4847.
(37) Peng, C.; Bernhard Schlegel, H. *Isr. J. Chem.* **1993**, *33*, 449−454.
(38) Peng, C.; Ayala, P. Y.; Schlegel, H. B.; Frisch, M. J. *J. Comput. Chem.* **1996**, *17*, 49−56.
(39) Domingo, L. R.; Perez, P. *Org. Biomol. Chem.* **2013**, *11*, 4350−4358.
(40) De Vleeschouwer, F.; Geerlings, P.; De Proft, F. *Theor. Chem. Acc.* **2012**, *131*, 1245.
(41) Minisci, F.; Vismara, E.; Fontana, F.; Morini, G.; Serravalle, M.; Giordano, C. *J. Org. Chem.* **1987**, *52*, 730−736.

DOI: 10.1021/acs.joc.6b00977
J. Org. Chem. 2016, 81, 7110−7120

(42) Minisci, F.; Vismara, E.; Morini, G.; Fontana, F.; Levi, S.; Serravalle, M.; Giordano, C. *J. Org. Chem.* **1986**, *51*, 476−479.
(43) Fujiwara, Y.; Dixon, J. A.; O'Hara, F.; Funder, E. D.; Dixon, D. D.; Rodriguez, R. A.; Baxter, R. D.; Herle, B.; Sach, N.; Collins, M. R.; Ishihara, Y.; Baran, P. S. *Nature* **2012**, *492*, 95−99.
(44) Frisch, M. J., et al. *Gaussian 09*, revision A.02, Gaussian, Inc., Wallingford, CT, 2009.
(45) Becke, A. D. *J. Chem. Phys.* **1993**, *98*, 5648−5652.
(46) Lee, C.; Yang, W.; Parr, R. G. *Phys. Rev. B: Condens. Matter Mater. Phys.* **1988**, *37*, 785−789.
(47) Stephens, P. J.; Devlin, F. J.; Chabalowski, C. F.; Frisch, M. J. *J. Phys. Chem.* **1994**, *98*, 11623−11627.
(48) Grimme, S.; Antony, J.; Ehrlich, S.; Krieg, H. *J. Chem. Phys.* **2010**, *132*, 154104.
(49) Grimme, S.; Ehrlich, S.; Goerigk, L. *J. Comput. Chem.* **2011**, *32*, 1456−1465.
(50) Baxter, R. D.; Liang, Y.; Hong, X.; Brown, T. A.; Zare, R. N.; Houk, K. N.; Baran, P. S.; Blackmond, D. G. *ACS Cent. Sci.* **2015**, *1*, 456−462.
(51) De Vleeschouwer, F.; Jaque, P.; Geerlings, P.; Toro-Labbé, A.; De Proft, F. *J. Org. Chem.* **2010**, *75*, 4964−4974.
(52) De Vleeschouwer, F.; Van Speybroeck, V.; Waroquier, M.; Geerlings, P.; De Proft, F. *Org. Lett.* **2007**, *9*, 2721−2724.
(53) Jayathilaka, P. B.; Pathiraja, G. C.; Bandara, A.; Subasinghe, N. D.; Nanayakkara, N. *Can. J. Chem.* **2014**, *92*, 809−813.
(54) Chai, J.-D.; Head-Gordon, M. *Phys. Chem. Chem. Phys.* **2008**, *10*, 6615−6620.
(55) Brémond, É.; Savarese, M.; Su, N. Q.; Pérez-Jiménez, Á. J.; Xu, X.; Sancho-García, J. C.; Adamo, C. *J. Chem. Theory Comput.* **2016**, *12*, 459−465.
(56) Xu, X.; Alecu, I. M.; Truhlar, D. G. *J. Chem. Theory Comput.* **2011**, *7*, 1667−1676.
(57) Jacquemin, D.; Perpète, E. A.; Ciofini, I.; Adamo, C. *Theor. Chem. Acc.* **2011**, *128*, 127−136.
(58) Jacquemin, D.; Mennucci, B.; Adamo, C. *Phys. Chem. Chem. Phys.* **2011**, *13*, 16987−16998.
(59) Krishnan, R.; Binkley, J. S.; Seeger, R.; Pople, J. A. *J. Chem. Phys.* **1980**, *72*, 650.
(60) Roy, L. E.; Hay, P. J.; Martin, R. L. *J. Chem. Theory Comput.* **2008**, *4*, 1029−1031.
(61) Tomasi, J.; Mennucci, B.; Cammi, R. *Chem. Rev.* **2005**, *105*, 2999−3094.
(62) Keith, T. A. TK Gristmill Software, Overland Park, KS, USA (aim.tkgristmill.com), 2016.
(63) Domingo, L. R.; Perez, P. *Org. Biomol. Chem.* **2011**, *9*, 7168−7175.

DOI: 10.1021/acs.joc.6b00977
J. Org. Chem. 2016, 81, 7110−7120